

Geophysical Research Letters®

RESEARCH LETTER

10.1029/2024GL109128

Key Points:

- Suspended macroalgal farms can enhance turbulence and drive upward nutrient fluxes from below the farm base to prevent starvation
- The Damkohler number, comparing nutrient transport with uptake by macroalgae, can be used to predict nutrient availability in the farm
- Farming strategies are proposed such as timely harvesting and selecting locations with a shallow nutricline and robust currents and waves

Supporting Information:

Supporting Information may be found in the online version of this article.

Correspondence to:

T. Bo,
tbo@atmos.ucla.edu

Citation:

Bo, T., McWilliams, J. C., Frieder, C. A., Davis, K. A., & Chamecki, M. (2024). Nutrient replenishment by turbulent mixing in suspended macroalgal farms. *Geophysical Research Letters*, 51, e2024GL109128. <https://doi.org/10.1029/2024GL109128>

Received 8 MAR 2024

Accepted 27 JUN 2024

Nutrient Replenishment by Turbulent Mixing in Suspended Macroalgal Farms



Tong Bo¹ , James C. McWilliams¹ , Christina A. Frieder² , Kristen A. Davis^{3,4} , and Marcelo Chamecki¹ 

¹Department of Atmospheric and Oceanic Sciences, University of California, Los Angeles, CA, USA, ²Southern California Coastal Water Research Project, Costa Mesa, CA, USA, ³Department of Civil and Environmental Engineering, University of California, Irvine, CA, USA, ⁴Department of Earth System Science, University of California, Irvine, CA, USA

Abstract This study uses large eddy simulations to investigate nutrient transport and uptake in suspended macroalgal farms. Various farm configurations and oceanic forcing conditions are examined, with the farm base located near the nutricline depth. We introduce the Damkohler number Da to quantify the balance between nutrient consumption by macroalgae uptake and supply by farm-enhanced nutrient transport. Most cases exhibit low Da , indicating that farm-generated turbulence drives sufficient upward nutrient fluxes, supporting macroalgae growth. High Da and starvation may occur in fully grown farm blocks, a configuration that generates the weakest turbulence, particularly when combined with densely planted macroalgae or weak flow conditions. Flow stagnation within the farm due to macroalgae drag may constrain the uptake efficiency and further increase the starvation risk. Mitigation strategies involve timely harvesting, avoiding dense macroalgae canopies, and selecting farm locations with robust ocean currents and waves. This study provides insights for sustainable macroalgal farm planning.

Plain Language Summary Offshore macroalgal farming has been proposed as a sustainable strategy for carbon sequestration, biofuel production, food supply, and bioremediation. However, challenges arise as macroalgal farms are typically suspended above the nutricline and may thus deplete the existing nutrient inventory near the sea surface. In this study, large eddy simulations reveal that suspended farms can generate intense turbulence and drive upward nutrient fluxes from below the farm base. Various farm simulations are conducted, and in most cases the farm-generated turbulence is indicated to provide sufficient nutrient fluxes to support macroalgae growth. This presents a self-sustaining solution for nutrient supply through passive entrainment. To mitigate the risk of farm starvation, we propose strategies such as timely harvesting, avoiding dense macroalgae canopies, and selecting farm locations with robust ocean currents and waves.

1. Introduction

Marine macroalgae play a vital role in maintaining ecosystem health by serving as crucial habitats and providing food sources for diverse marine species (e.g., Dayton, 1985; Teagle et al., 2017). Beyond their ecological importance, the cultivation of macroalgae has been proposed as a sustainable strategy for carbon sequestration, biofuel production, food supply, and bioremediation (Arzeno-Soltero et al., 2023; Ferdouse et al., 2018; Ghadiryanfar et al., 2016). Recent interest has grown in expanding macroalgal farming offshore utilizing suspended structures, due to difficulty of permitting and competing uses for shallow, nearshore coastal regions (Arzeno-Soltero et al., 2023; Fernand et al., 2017; Frieder et al., 2022; Troell et al., 2009).

Suspended macroalgal farms are typically located within the upper mixed layer of the ocean. A crucial factor affecting farm performance is the interaction of suspended farms with hydrodynamic processes in the mixed layer (Frieder et al., 2022; Yan et al., 2021). Macroalgae exert drag forces on the flow, causing current and wave attenuation (Jackson, 1997; Monismith et al., 2022; Rosman et al., 2007; Thom, 1971). Discontinuities in drag can lead to the development of shear layers and eddies at the edges of the farm (Plew, 2011; Yan et al., 2021). In addition, enhanced Langmuir-type circulations can be created within farms due to the interplay between surface gravity waves and farm-modulated currents (Bo et al., 2024; Yan et al., 2021). Moreover, these farm-generated hydrodynamic processes also exhibit a distinct dependence on details of farm design such as farm geometry and biomass density (Bailey & Stoll, 2013; Bo et al., 2024; Poggi et al., 2004). The varied hydrodynamic responses associated with different farm configurations can consequently result in various impacts on the mixing and transport of chemicals and nutrients.

© 2024. The Author(s).

This is an open access article under the terms of the Creative Commons Attribution License, which permits use, distribution and reproduction in any medium, provided the original work is properly cited.

Optimal farm design ensures an adequate nutrient supply for cultivated macroalgae throughout the canopy. Suspended farms are usually positioned near the sea surface to maximize light exposure and allow for easier harvesting (Arzeno-Soltero et al., 2023; Frieder et al., 2022). However, challenges arise because of the relatively low nutrient concentrations near the surface. Farm starvation may occur in two scenarios: (a) a complete absence of background nutrients in the mixed layer caused by larger scale ocean dynamics and biogeochemistry, where the concentration is below the criteria for farm growth, or (b) when there is initially sufficient background nutrient, but rapid macroalgal consumption depletes the existing nutrient within the farm. Turbulence and coherent eddies generated by these farms have the potential to induce significant vertical mixing (Abdolahpour et al., 2017; Nepf et al., 2007; Yan et al., 2021), leading to the consistent entrainment of nutrients from below the farm base to prevent starvation. This introduces a self-sustaining mechanism for passive nutrient supply to the farm (Frieder et al., 2022). Considering the variability of farm-generated turbulence associated with distinct farm configurations (Bo et al., 2024; Yan et al., 2021), further investigation into nutrient transport and uptake by the farm is therefore essential for optimally designing farm layouts to ensure nutrient availability and support macroalgae growth.

This study uses large eddy simulations (LES) to investigate nutrient transport and uptake associated with suspended macroalgal farms, aiming to understand the hydrodynamic aspects influencing nutrient availability for farm growth. Section 2 describes the numerical approach and the various farm simulations examined in this study. In Section 3, we analyze farm-generated turbulence and nutrient fluxes across different simulations. We also investigate nutrient uptake associated with varied farm configurations, and compare the relative impacts of nutrient uptake versus turbulent transport in determining nutrient availability. Section 4 discusses potential factors affecting farm performance and concludes the study.

2. Methods

2.1. LES Model Description

The LES method (Deardorff, 1970; Smagorinsky, 1963) is used to study the hydrodynamics, nutrient transport, and nutrient uptake for farms of giant kelp (*Macrocystis pyrifera*). We choose to use LES as it can effectively capture the intricate mixing processes driven by farm-generated turbulence. The LES framework is based on a set of wave-averaged and grid-filtered equations for velocity, temperature, and passive tracer (see Text S1 in Supporting Information S1 for details). Specifically, the Craik–Leibovich vortex force and Coriolis force are included to represent the influences of surface gravity waves and planetary rotation (Craik & Leibovich, 1976; McWilliams et al., 1997). The code has been validated and used in previous macroalgal farm and boundary layer flow studies (Bo et al., 2024; Yan et al., 2021, 2022).

The resistance imposed by kelp onto the flow is parameterized as a drag force F_D in the momentum equation, and is expressed as

$$\mathbf{F}_D = \frac{1}{2} C_D a(z) \mathbf{P} \cdot (\mathbf{u} |\mathbf{u}|). \quad (1)$$

The velocity vector is $\mathbf{u} = (u, v, w)$, including the streamwise (x), cross-stream (y), and vertical (z) components, respectively. The term $a(z)$ is the depth-dependent frond surface area density (surface area per unit volume, m^{-1}) obtained by conversion of the algal biomass (Frieder et al., 2022). The drag coefficient $C_D = 0.0148$ is based on the experimental study by Utter and Denny (1996). While the empirical fit in Utter and Denny (1996) for a broad range of flow speeds suggests a best-fit velocity exponent of 1.596, the traditional quadratic drag law in Equation 1 provides a similarly effective representation of their measurements for the flow speeds used in our study (below 1 m/s). Our results show minimal sensitivity to the choice of drag model (see Text S2 in Supporting Information S1). The coefficient tensor \mathbf{P} stands for the projection of frond surface area into each direction. Although the projection can be directionally dependent due to the geometry of kelp fronds, we use an isotropic projection of $\mathbf{P} = (1/2)\mathbf{I}$ for simplicity, where \mathbf{I} is the identity matrix (Yan et al., 2021). We assume that kelp fronds and stipes passively follow wave motion, so wave orbital velocity is not included in Equation 1 and the interaction between wave and canopy drag is not considered.

Nutrients are treated as a passive tracer in the model, and in particular we focus on nitrate in this study as it is the limiting macronutrient in many regions where *Macrocystis pyrifera* grows. Nutrient uptake by kelp is treated as a sink term S in the tracer transport equation (Text S1 in Supporting Information S1), written as

$$S = a(z)V_{\max} \frac{N}{N + K_M}. \quad (2)$$

This is the Michaelis-Menten formula (Cornish-Bowden, 2015; Michaelis & Menten, 1913), where the uptake rate saturates and approaches the maximum value V_{\max} as nitrate concentration N increases. Here, $K_M = 10.2 \mu\text{M}$ (micromolar) is the half saturation constant of nitrate for *Macrocystis pyrifera*. Previous studies have reported V_{\max} values varying from 0.03 to 0.4 $\mu\text{mol m}^{-2}\text{s}^{-1}$ (Arzeno-Soltero et al., 2023; Frieder et al., 2022; Gerard, 1982; Haines & Wheeler, 1978), and in this study $V_{\max} = 0.2 \mu\text{mol m}^{-2}\text{s}^{-1}$ is used as a representative value. Additional simulations are conducted with V_{\max} increased by a factor of three to investigate a scenario with a high uptake rate (Arzeno-Soltero et al., 2023).

The potential dependence of uptake on flow speed is examined by adding a velocity factor $F(|\mathbf{u}|)$ to the Michaelis-Menten formula (Broch & Slagstad, 2012), that is,

$$S = a(z)V_{\max} \frac{N}{N + K_M} F(|\mathbf{u}|) = a(z)V_{\max} \frac{N}{N + K_M} \left[1 - \exp\left(-\frac{|\mathbf{u}|}{u_{ref}}\right) \right]. \quad (3)$$

The rationale behind this velocity factor is that, at low velocities, the thick diffusive boundary layers surrounding kelp fronds pose constraints on the nutrient uptake rate (Huang et al., 2011; Stevens & Hurd, 1997). In contrast, at higher velocities the boundary layer thickness is no longer a limiting factor, and Equation 3 approaches the Michaelis-Menten formula in Equation 2. The reference velocity $u_{ref} = 0.03 \text{ m s}^{-1}$ (Broch & Slagstad, 2012; Stevens & Hurd, 1997) corresponds to the velocity at which the uptake reaches 65% of the optimal rate.

The periodic stripping of the diffusive boundary layer by waves can increase the nutrient uptake rate, particularly under weak current conditions (Frieder et al., 2022; Stevens & Hurd, 1997). Moreover, the flapping of kelp fronds in currents can lead to vortex shedding, stripping away the diffusive boundary layer and enhancing the nutrient flux to the kelp (Huang et al., 2011). Using more intricate formulas, for example, by explicitly incorporating the wave frequency and kelp flapping frequency could introduce additional variability in the uptake rate, but here for simplicity we use the empirical velocity dependence formula in Equation 3 from Stevens and Hurd (1997) and Broch and Slagstad (2012). This is consistent with the assumption in the momentum equation that kelp passively moves with the waves.

2.2. Farm Simulation Setup

The cultivation of macroalgae in open ocean environments involves a diverse range of aquaculture structures. A representative farm configuration considered here consists of a series of organized longlines spaced horizontally (Frieder et al., 2022; Yan et al., 2021). Each longline is deployed at a constant depth, anchored at both ends and also connected to surface buoys. *Macrocystis pyrifera* is cultivated along growth ropes attached to the longlines, and will grow upright toward the surface due to their buoyancy.

Macroalgal farm simulations are conducted on a $800 \times 208 \times 120 \text{ m}^3$ domain, with $400 \times 104 \times 240$ uniformly distributed grid cells. A turbulent flow undisturbed by the presence of the farm is input from the upstream boundary, and the analyses focus on a period during which the background flow has fully adapted to the presence of the suspended farm (details provided in Supporting Information S1). The farm is located in the middle of the domain from $x = 0$ to $x = L_f$, with a farm length of $L_f = 400 \text{ m}$ (Figure 1d). The upstream boundary is at $x = -150 \text{ m}$, and the downstream boundary is at a distance of 250 m from the farm trailing edge. In the y -direction the farm extends across the entire domain with a periodic boundary, that is, effectively assuming an infinite farm width. In the vertical direction the farm is between the sea surface and $h_b = -20 \text{ m}$ (the farm base), that is, the depth at which the suspended longlines are deployed. The farm structure is assumed to maintain a fixed location in the flow, with kelp exhibiting only small-amplitude oscillations passively following the wave orbital motion.

Two types of horizontal farm arrangements are examined (Figure 1f). The first arrangement consists of spaced longlines (farm rows) aligned parallel to the x -direction, extending the length of the farm. The second arrangement features kelp rows deployed close together, such that gaps between the rows are small enough to avoid significant impact on flow dynamics, essentially forming a horizontally uniform farm block. From a

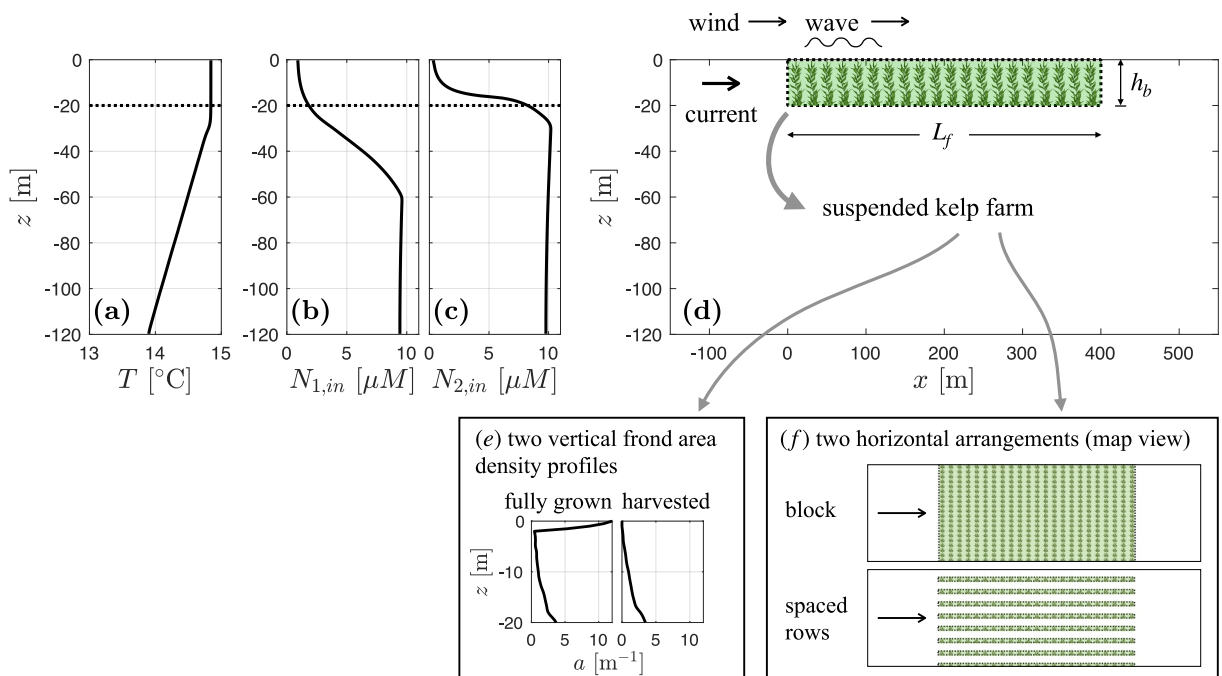


Figure 1. Simulation setup. (a): Temperature profile at the upstream boundary (inflow condition). (b) and (c): Two inflow nutrient profiles. Dotted black lines indicate the farm base. (d): A schematic of the farm simulation (side view), with vertical profiles of frond area density (e) and map views of farm configurations (f) in the auxiliary subfigures. Harvest practices typically focus on the uppermost 1–2 m of the farm, resulting in a frond area density of zero near the sea surface in the harvested profile.

hydrodynamics perspective, this block configuration is also representative of the scenario where longlines are deployed perpendicular to the x -direction (Bo et al., 2024).

In addition, two vertical profiles of frond surface area density $a(z)$ are considered (Figure 1e), representing two different growth stages of kelp (Frieder et al., 2022): (a) a fully grown profile, where kelp extends from the farm base to the sea surface, with high frond area density at the top due to a large portion of the fronds floating at the sea surface; (b) a harvested profile, where the frond density is reduced to zero in the uppermost 1–2 m part of the farm near the sea surface, as a result of harvest practices. The frond surface area density profiles of the two stages are obtained by conversion of the algal biomass (Frieder et al., 2022), with depth-averaged values of 2 m^{-1} and 1 m^{-1} , respectively. Additional simulations are performed in which these profiles of frond surface area are multiplied by a factor of 0.3 or 3, to investigate the influence of decreasing or increasing the kelp density within the farm.

The ocean forcing conditions are generally the same as those in McWilliams et al. (1997), Yan et al. (2021), and Bo et al. (2024). A geostrophic current $u_g = 0.2 \text{ m s}^{-1}$ is imposed in x -direction, representing the effect of mesoscale flow. The Coriolis frequency $f = 10^{-4} \text{ s}^{-1}$ corresponds to around 45°N latitude. A constant wind stress $\tau_w = 0.037 \text{ N m}^{-2}$ is applied at the sea surface, corresponding to a wind speed at 10-m height above the surface of 5 m s^{-1} . A monochromatic surface wave field with amplitude $A_w = 0.80 \text{ m}$ and the wavelength $\lambda_w = 60 \text{ m}$ is considered. Note that the effects of waves are incorporated in the model by imposing the Stokes drift, rather than explicitly resolving the free surface (details in Supporting Information S1). In addition, we explore another set of weaker current, wind, and wave conditions to investigate variability in ocean conditions, where $u_g = 0.05 \text{ m s}^{-1}$, $\tau_w = 0.009 \text{ N m}^{-2}$, and $A_w = 0.57 \text{ m}$.

The initial mixed layer depth at the upstream boundary (inflow) is 25 m (Figure 1a), and a stably stratified layer is beneath it, with a uniform temperature gradient $dT/dz = 0.01^\circ \text{C m}^{-1}$. We assume no heat flux at the surface boundary. Two background (inflow) nutrient profiles are examined in this study. The first profile (N_1) is a representative nutrient condition from the California Current System model (Deutsch et al., 2021; Frieder et al., 2022; Renault et al., 2021), featuring a relatively weak vertical gradient within the mixed layer, a strong gradient below the mixed layer (considered as a nutricline), and a uniformly high concentration of around $10 \mu\text{M}$ below 60 m (Figure 1b). The second profile (N_2) exhibits a relatively strong vertical gradient within the mixed

layer and a uniform concentration of 10 μM below the mixed layer (Figure 1c), representing a scenario with a shallower nutricline.

More detailed descriptions of simulation setup and farm configurations are provided in Supporting Information S1. Note that this study does not delve into the intricate mechanisms of how various farm configurations and ocean conditions lead to distinct hydrodynamics and nutrient mixing; these aspects were addressed in a prior study by Bo et al. (2024). Instead, our major objective in conducting a range of farm simulations is to generate variable levels of nutrient mixing and uptake and to examine how their balance influences nutrient availability within the farm.

3. Results

In this section we present the hydrodynamics, nutrient transport, and uptake associated with the kelp farm. Previous studies indicate that suspended farms can generate both standing eddies (secondary circulations, also known as attached Langmuir cells) and temporally fluctuating turbulence (Bo et al., 2024; Yan et al., 2021). Here we introduce a flow decomposition to separate distinct flow components and quantify their respective contributions to nutrient transport. The instantaneous flow field can be split into the mean flow, standing eddies, and turbulence, that is,

$$\mathbf{u} = \langle \overline{\mathbf{u}} \rangle_y + \overline{\mathbf{u}^s} + \mathbf{u}' \quad (4)$$

The overline represents the time average, and the prime represents temporal fluctuations around the time average, that is, the turbulent component. Here $\langle \cdot \rangle_y$ denotes the cross-stream average, and the superscript “s” denotes the standing-eddy component (time-averaged spatial variations in y -direction generated by the farm structure). Similarly, the covariance between velocity and nutrient concentration can be decomposed as

$$\langle \overline{\mathbf{u}N} \rangle_y = \langle \overline{\mathbf{u}} \rangle_y \langle \overline{N} \rangle_y + \langle \overline{\mathbf{u}^s N^s} \rangle_y + \left\langle \overline{\mathbf{u}' N'} \right\rangle_y \quad (5)$$

The second term on the right side stands for the cross-stream-averaged nutrient transport driven by the standing eddy, effectively a dispersive flux (Finnigan, 2000), and the third term represents the turbulent flux.

3.1. Farm-Enhanced Boundary Layer Eddies

As ocean currents enter the farm, the mean flow is decelerated due to the drag force exerted by the kelp. The kelp drag discontinuity at the farm bottom edge enhances the vertical shear of streamwise velocity, leading to the development of shear layer eddies (Figure 2a). Here we specifically consider the vertical component w' when discussing turbulence intensity, because of its direct relevance to vertical transport in kelp farms. Moreover, Langmuir-type turbulence is generated within the farm due to the combined effects of waves and farm-modulated currents (Bo et al., 2024; Yan et al., 2021). The farm-generated Langmuir turbulence exhibits a stronger magnitude compared to the standard Langmuir turbulence in the upstream region, which typically occurs in the surface boundary layer without the presence of kelp (McWilliams et al., 1997). In addition to turbulence, standing eddies occur exclusively in farm configurations with horizontally spaced kelp rows (Bo et al., 2024; Yan et al., 2021) (Figure 2b). The strength of the farm-generated turbulence and standing eddies varies with farm configurations and oceanic forcing conditions (Bo et al., 2024), and these variations lead to different vertical transport of nutrients, as detailed in the subsequent section.

3.2. Vertical Nutrient Transport

Both farm-generated turbulence and standing eddies can drive upward nutrient fluxes (Figures 2c and 2d). To quantify the strength of farm-generated vertical mixing, we define the turbulent and standing-eddy mixing coefficients (κ_t and κ_s) based on the cross-stream-averaged fluxes in Equation 5,

$$\kappa_t = \frac{\left\langle \overline{w' N'} \right\rangle_y}{d\langle \overline{N} \rangle_y / dz}, \quad (6a)$$

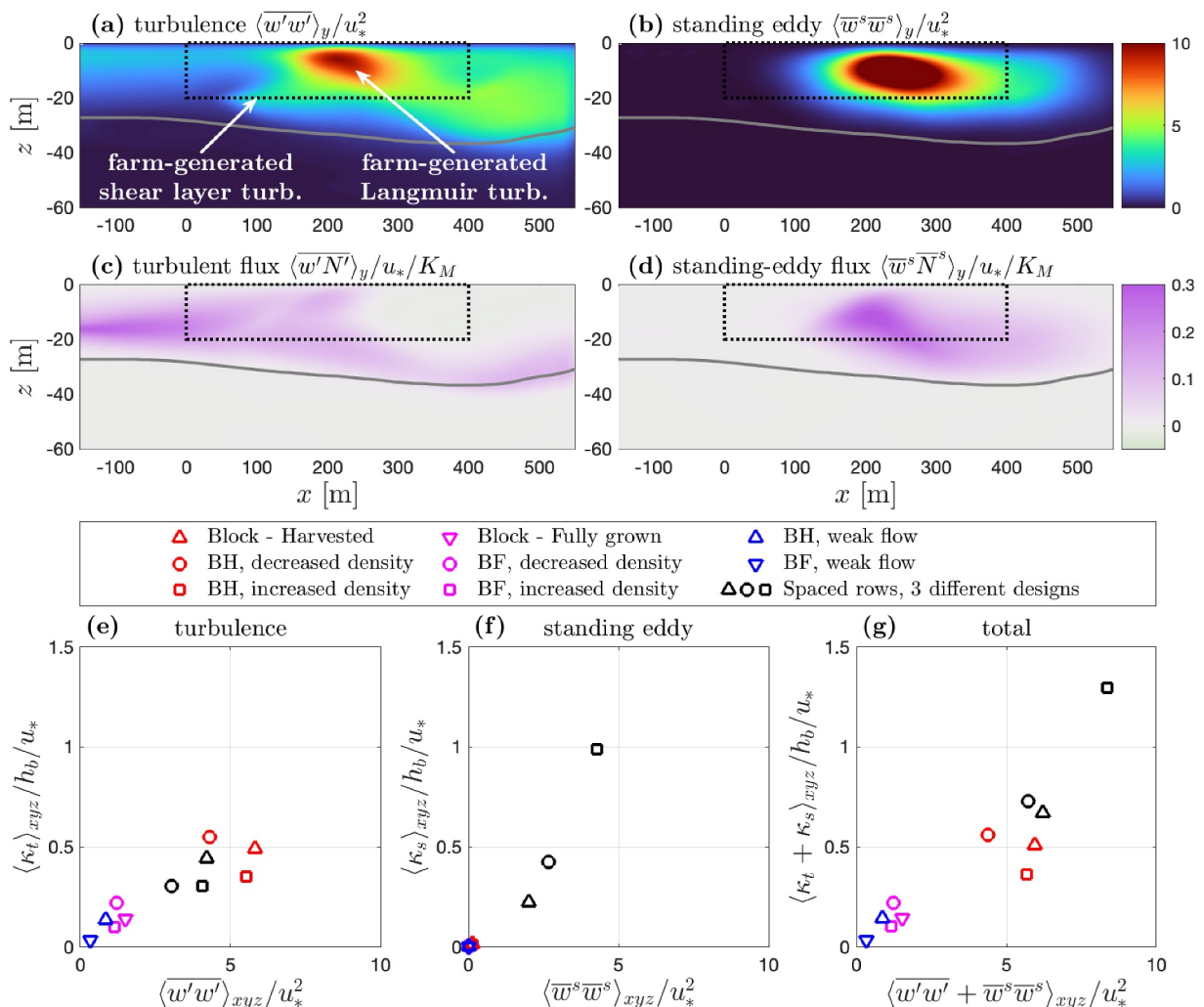


Figure 2. Eddies and nutrient fluxes associated with the kelp farm, in a simulation with horizontally spaced kelp rows. (a) and (b): Side views of turbulence and standing eddy intensity (the vertical component). Dotted rectangles show the extent of the farm, and the solid gray lines represent the mixed layer depth. Here the mixed layer depth is defined as the minimum depth at which the laterally averaged temperature deviates from the sea surface temperature by 0.1°C . (c) and (d): Side views of vertical nutrient fluxes driven by turbulence and standing eddies for profile N_2 . (e)–(g): Turbulent (e), standing-eddy (f), and total (g) mixing coefficients versus turbulence or eddy intensity (averaged within the farm) for various simulations. The detailed parameters for different simulations can be found in Table S1 in Supporting Information S1.

$$\kappa_s = \frac{\langle \bar{w}^s\bar{N}^s \rangle_y}{d\langle N \rangle_y / dz}. \quad (6b)$$

The mixing coefficients calculated with the two nutrient profiles N_1 and N_2 are generally consistent, and we use profile N_2 for the calculation of mixing coefficients, because its stronger vertical gradients on the denominator provide more robust results.

More in-depth analyses of how various farm configurations lead to distinct turbulence intensities have been conducted by Bo et al. (2024), and we provide a concise summary here. In spaced kelp rows aligned with the background current, both turbulence and standing eddies occur irrespective of the vertical kelp frond density distribution, leading to large nutrient fluxes (Figures 2e and 2f). In contrast, standing eddies do not form in farm blocks. Relatively strong turbulence and nutrient mixing are found in farm blocks with a harvested profile, while turbulent mixing is weak in cases with a fully grown profile due to an inhibition of Langmuir turbulence by the

large frond area density near the ocean surface (Bo et al., 2024). Additionally, turbulence intensity and mixing decrease in simulations with weaker currents and waves.

The mixing coefficients generally exhibit a positive correlation with the corresponding turbulence (or eddy) intensity across various simulations (Figures 2e–2g). This is in agreement with the mixing length theory, where the mixing coefficient scales with the eddy velocity-scale multiplied by a length-scale. The mixing length for turbulence appears to be much smaller than the farm height (approximately $0.2h_b$), consistent with findings by Abdolahpour et al. (2017). The standing-eddy mixing coefficient has a steeper slope dependence on eddy intensity than the turbulent mixing coefficient, indicating that the standing eddies responsible for driving nutrient fluxes have a larger length-scale (up to $0.5h_b$) compared to that of turbulence.

3.3. Nutrient Supply Versus Uptake

While farm-generated turbulence can lead to upward fluxes that increase nutrient availability in the farm, kelp uptake consumes nutrients and may thus result in nutrient depletion and kelp starvation. In this section, we consider the Michaelis-Menten uptake formula in Equation 2 and compare the influence of nutrient uptake to nutrient fluxes. We define a farm-averaged Damkohler number (e.g., Rehage & Kind, 2021)

$$Da = \frac{\tau_{mix}}{\tau_{uptake}} = \frac{\langle a \rangle_{xyz} V_{max} h_b^2}{\langle \kappa_t + \kappa_s \rangle_{xyz} K_M}, \quad (7)$$

which compares the mixing timescale $\tau_{mix} = h_b^2 / \langle \kappa_t + \kappa_s \rangle_{xyz}$ with the uptake timescale $\tau_{uptake} = K_M / (\langle a \rangle_{xyz} V_{max})$. Note that the frond area density a and the turbulent and standing-eddy mixing coefficients κ_t and κ_s vary with farm configurations. Da effectively quantifies the relative strength of nutrient consumption by the farm and the supply by vertical mixing, with $Da \ll 1$ indicating cases with supply larger than consumption, and vice versa for $Da \gg 1$.

The Damkohler number Da demonstrates a clear correlation with nutrient availability in the farm, which is quantified here as a dimensionless uptake efficiency $S/a/V_{max}$ (Figure 3a). This dimensionless uptake efficiency represents the ratio of the actual nutrient uptake rate to its potential maximum at saturating nutrient concentration (i.e., for $N \gg K_M$ in Equation 2). The uptake efficiency is bounded between 0 and 1 by definition, and in our simulations its upper limit is typically well below 1 because the uptake rate rarely reaches its potential maximum. For low values of Da , nutrient entrainment from below the farm exceeds the consumption rate, ensuring adequate nutrients and high uptake efficiency to support kelp growth. In this scenario, nutrient concentration is increased at the farm exit compared to the background nutrient profile entering the farm (Figures 3b and 3d).

In contrast, for high Da , farm-generated nutrient fluxes are insufficient to balance uptake, resulting in nutrient depletion at the farm exit (Figures 3c and 3d) and potentially leading to the threat of starvation. The transition to starvation, estimated by applying the threshold of 1 μM nitrate (Zimmerman & Kremer, 1984) (ZK1984) to the Michaelis-Menten formula, occurs at around $Da = 1$ (Figure 3a). It is also important to note that the ZK1984 value should only be viewed as a general reference. While higher Da and lower nutrient uptake efficiency typically indicate an increased risk of starvation, falling below the ZK1984 value does not necessarily result in starvation.

The above analysis is based on the first nutrient profile (N_1 , obtained from California Current System model). The dependence of uptake efficiency on Da also holds for the other nutrient profile (N_2 , with stronger vertical gradients near the sea surface, Figures 3e–3h), except that the variability in uptake efficiency is much greater than that for N_1 . This is because N_2 has a greater range of nutrient concentration within the surface boundary layer. The transition to starvation occurs at a larger Da (around 5) for profile N_2 .

For nutrient profiles N_1 and N_2 , most cases exhibit a small Da , suggesting that farm-generated fluxes can provide adequate nutrients to prevent starvation. Nutrient depletion and high Da are most likely to occur in farm blocks with a fully grown profile, that is, the farm configuration with the least turbulence generation, in particular when this configuration is combined with dense kelp that increases the uptake rate or weak current and wave conditions that decreases vertical nutrient mixing. Note that the farm blocks typically have a larger farm-averaged frond density $\langle a \rangle_{xyz}$ than spaced rows. However, the increase in Da for farm blocks is beyond that predicted by the increase in $\langle a \rangle_{xyz}$ alone, indicating that weakened vertical mixing due to the farm configuration is also a significant contributor to lower nutrient availability. While in most cases the high uptake rate is attributed to the

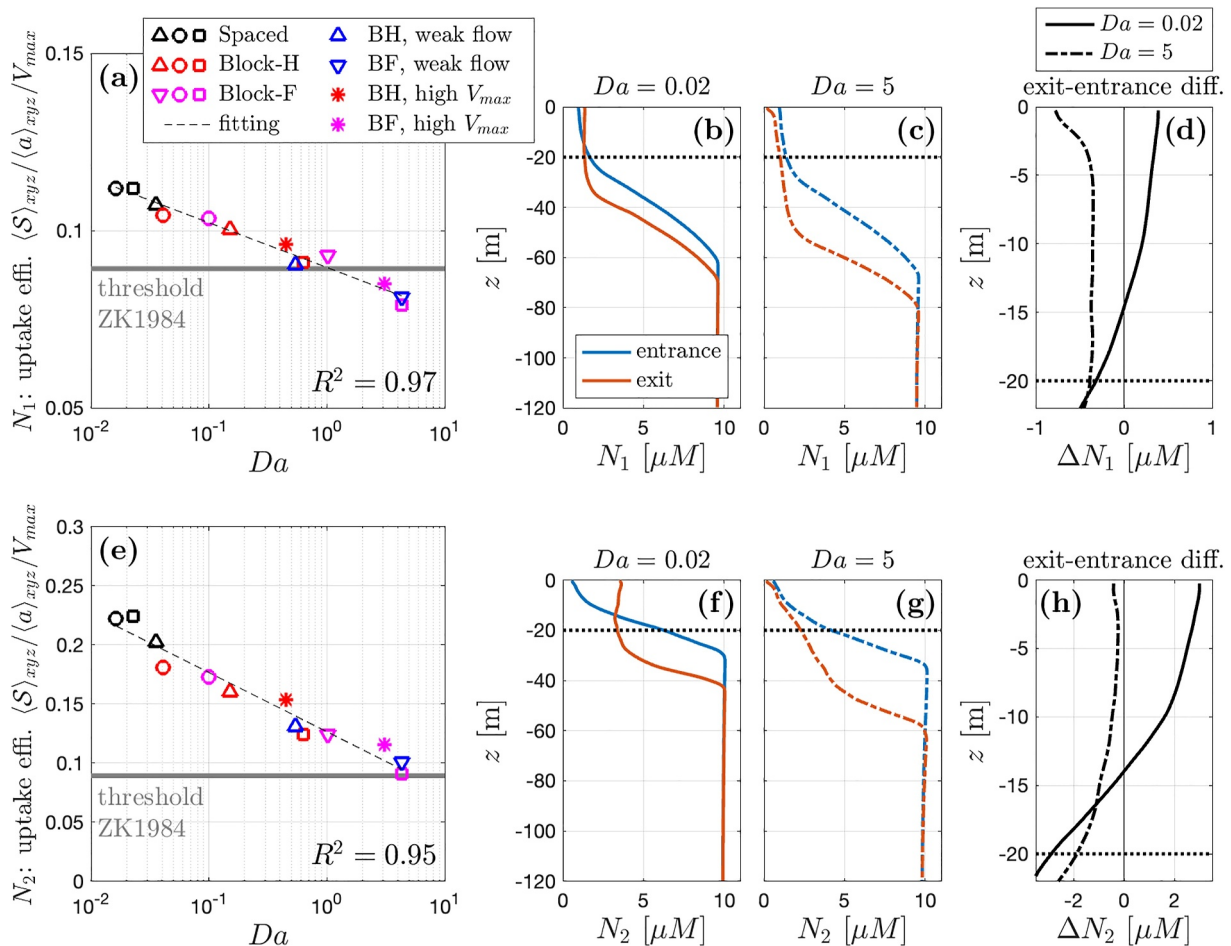


Figure 3. Dependence of farm nutrient availability on Da . (a): Uptake efficiency versus Da across different simulations, for nutrient profile N_1 (Figure 1b). Case symbols are consistent with Figure 2. The horizontal gray line is the estimated threshold for kelp growth according to Zimmerman and Kremer (1984). (b) and (c): Vertical nutrient profiles at the farm entrance and exit, for simulations with a low and high Da ($Da = 0.02$ and $Da = 5$), respectively. (d): Exit-entrance difference for low and high Da . (e)–(h): A similar set of plots for nutrient profile N_2 (Figure 1c).

increased $\langle a \rangle_{xyz}$, two additional simulations with an increased V_{max} also lead to a high uptake rate and reduced nutrient availability, similar to the effect of the increased $\langle a \rangle_{xyz}$.

Moreover, additional analysis is included in Supporting Information (Text S3 in Supporting Information S1) on how the correlation between uptake efficiency and Da varies with background nutrient profiles. Overall Da proves to be an effective metric for predicting nutrient uptake. In order to assess the importance of farm-generated turbulence for nutrient availability, another simulation is conducted for a harvested farm block while setting C_D to 0, that is, effectively removing drag and farm-generated turbulence but maintaining the nutrient uptake by the farm. This simulation shows weaker nutrient mixing, higher Da , and decreased uptake efficiency (20% decrease for profile N_1 and 40% decrease for profile N_2 , not shown), further demonstrating the crucial role of farm-generated turbulence in driving nutrient supply.

It is also worth noting that other scenarios for starvation may occur, such as when the nutricline is substantially below the farm base, with a complete absence of nutrients in the mixed layer. This starvation regime is not the focus of the present study, as the farm-generated turbulence would be incapable of transporting nutrients from the deep nutricline. In addition, stronger stratification near the ocean surface boundary can inhibit vertical mixing and limit the upward supply of nutrients (discussed in detail in Text S4 in Supporting Information S1).

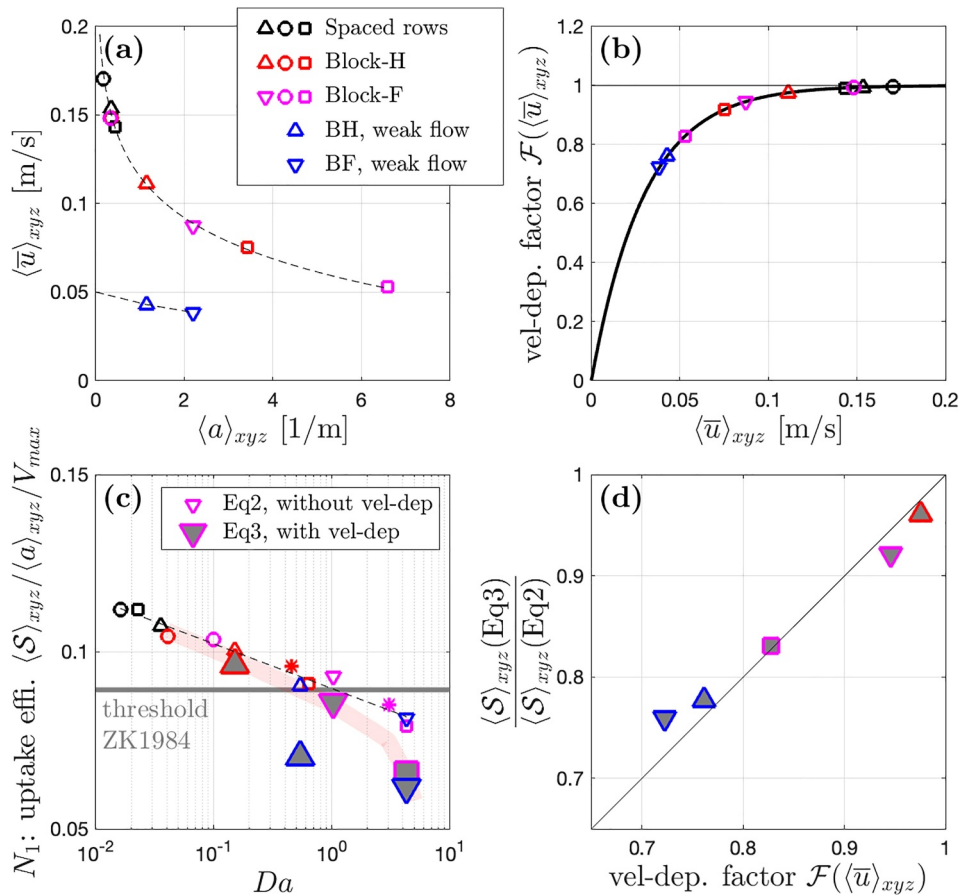


Figure 4. Influences of hydrodynamic conditions on nutrient uptake. (a): Average streamwise velocity within the farm versus average kelp frond area density. Case symbols are consistent with Figures 2 and 3. (b): The velocity dependence factor in Equation 3 as a function of mean flow speed. (c): Uptake efficiency versus Da for nutrient profile N_1 . Gray-filled markers represents simulations that incorporate the velocity-dependence of uptake rate based on Equation 3, and the other simulations based on Equation 2 do not have this velocity-dependence. (d): The decrease in uptake efficiency due to velocity constraints (ratio of uptake efficiency, with vs. without velocity-dependence in subfigure (c)), compared with the velocity-dependence factor from subfigure (b). Only profile N_1 is shown as an example here, and profile N_2 yields consistent results.

3.4. Dependence of Uptake on Hydrodynamic Conditions

The dependency of kelp uptake rate on hydrodynamic conditions is another critical aspect that, alongside the factors mentioned above, may lead to kelp starvation. In this section, we investigate the modified Michaelis-Menten uptake formula that integrates the influence of velocity (Equation 3). The drag exerted by kelp tends to decelerate the mean current within the farm, and this deceleration is particularly pronounced in dense farms (Figure 4a). The decreased velocity results in thicker diffusive boundary layers around kelp fronds, resulting in an additional constraint on kelp nutrient uptake (Stevens & Hurd, 1997).

The reduction in uptake rate due to low flow speeds is most notable in cases with weak background ocean currents or high kelp density, both of which can decrease the mean velocity in the farm to less than $\sim 0.05 \text{ m s}^{-1}$. The velocity constraint factor $\mathcal{F}(|\bar{u}|)$ in Equation 3 can thus be decreased to approximately 0.7 (Figure 4b), leading to a decrease of up to 30% in uptake efficiency (Figure 4c). Moreover, these cases characterized by reduced flow speeds coincide with high Da values as investigated in the previous section. Consequently, the velocity constraint further increases the risk of starvation posed by the low nutrient availability. The uptake efficiency converges toward that obtained by the standard Michaelis-Menten formula in other cases where velocity remains higher than $\sim 0.05 \text{ m s}^{-1}$ within the farm.

Additionally, the relative reduction in uptake efficiency generally aligns with the velocity-dependence factor calculated from the bulk average streamwise velocity (Figure 4d). This suggests that the spatial and temporal

variability of velocity within the farm has minimal influences on the overall uptake, and using the farm-averaged mean velocity is sufficient for predicting the reduced uptake due to the formation of thick diffusive boundary layers.

4. Discussion and Conclusion

This study investigates the impacts of vertical nutrient fluxes and kelp uptake on nutrient availability in the farm, and the Damkohler number Da is introduced to quantify the competing effects of the two processes. Most investigated farm configurations exhibit a small Da , indicating that farm-generated turbulence can provide sufficient nutrient supply to exceed kelp uptake. This supports the concept of a self-sustaining solution for nutrient supply to the farm through passive entrainment. It is noteworthy that Langmuir-type turbulence usually prevails over shear layer turbulence within the farm, emphasizing the role of wave-current interaction in creating vertical fluxes and preventing nutrient depletion. Starvation and high Da are most likely to occur in farm blocks with the fully grown profile, caused by increased nutrient consumption due to high kelp density and decreased vertical mixing due to inhibited turbulence in this farm configuration. Additionally, when the spaced kelp rows are oriented perpendicular to the flow direction, the turbulence intensity is demonstrated to be similar to that of farm blocks (Bo et al., 2024). Therefore, nutrient transport in farm blocks is also indicative of farms with rows perpendicular to the flow.

Several strategies for farm development are proposed to prevent starvation. Timely harvesting can prevent the formation of a fully grown profile, favoring turbulence generation within the farm and ensuring nutrient supply from deeper waters. Densely planted kelp should be avoided, as high frond density can not only increase nutrient consumption, but also lead to flow stagnation in the farm, constraining uptake efficiency and potentially causing kelp starvation. Deploying farms in regions with strong ocean currents and waves can enhance turbulence generation, ensuring nutrient availability. Additionally, selecting a location where the nutricline is relatively shallow, for example, comparable to the farm base depth, is recommended, so that farm-generated turbulence has the potential to induce the upward nutrient transport.

The Damkohler number Da provides a predictive tool for potential nutrient depletion in the context of farm planning. Accurate calculation of the mixing coefficient is crucial for obtaining a reliable Da . The calculation can be achieved by using hydrodynamic models capable of resolving vertical nutrient transport through the farm. Alternatively, our simulations revealed a positive correlation between the mixing coefficient and turbulence intensity, consistent with the classical mixing length theory. Predicting uptake efficiency based on turbulence intensity thus becomes feasible, which connects to the previous findings on the dependence of turbulence intensity on various farm configurations (Bo et al., 2024).

While we focused on a 400 m farm length, implications of starvation can be extended to longer or infinite farms under similar ocean and nutrient conditions by using Da . In high Da cases, nutrient concentration is expected to decay downstream along the farm, leading to depletion after a distance comparable to the uptake timescale multiplied by mean streamwise velocity. Larger values of Da thus indicate occurrence of depletion over a shorter distance, increasing the risk of starvation. The farms investigated here have an infinite width due to periodic boundary conditions in the y -direction, serving as a suitable proxy for wide farms. We also note that additional standing eddies can be generated on the cross-stream edges of farms with finite width (Tseung et al., 2016), thereby affecting nutrient transport.

Moreover, the correlation between uptake efficiency and Da can vary with different background nutrient profiles. The negative dependence of uptake efficiency on Da remains consistent across a range of nutrient profiles, though the threshold value is not always around $Da = 1$, as found in profiles $N1$ and $N2$. In general, the slope of the negative correlation becomes steeper as vertical nutrient concentration gradients increase, while the intercept increases with higher average nutrient concentration in the mixed layer. This suggests that the slope and intercept of the correlation, as well as the threshold Da value, can potentially be predicted based on a given background nutrient concentration (details provided in Text S3 in Supporting Information S1).

This study mainly examines scenarios where the nutricline depth is comparable to the farm base depth. Scenarios where the nutricline is substantially below the farm are not the central focus, as this may inevitably lead to starvation given that farm-generated turbulence would be unable to drive nutrient fluxes from the deep nutricline. In addition, the stratification condition examined here is typically relevant for offshore farming, whereas in

coastal waters the surface ocean can be more stratified. Strong stratification near the surface boundary can inhibit vertical mixing (Plew et al., 2006), thus increasing the risk of nutrient depletion (Text S4 in Supporting Information S1). Furthermore, while this study primarily investigates hydrodynamic transport processes affecting nutrient availability, other factors, such as the impact of high temperature on kelp growth, represent additional threats, particularly during El Niño years.

Data Availability Statement

Model data generated in this study are available at Zenodo repository at Bo (2024).

Acknowledgments

This project was funded by the U.S. Department of Energy ARPA-E MARINER (Macroalgae Research Inspiring Novel Energy Resources) program, Grant DE-AR0000920. The authors acknowledge high-performance computing support from Derecho (<https://doi.org/10.5065/qx9a-pg09>) provided by NCAR's Computational and Information Systems Laboratory, sponsored by the National Science Foundation. The authors thank Chao Yan, Daniel Dauhajre, and Daniele Bianchi for helpful discussions, and thank two anonymous reviewers for their valuable comments.

References

- Abdolahpour, M., Ghisalberti, M., Lavery, P., & McMahon, K. (2017). Vertical mixing in coastal canopies. *Limnology & Oceanography*, 62(1), 26–42. <https://doi.org/10.1002/lno.10368>
- Arzeno-Soltero, I. B., Saenz, B. T., Frieder, C. A., Long, M. C., DeAngelo, J., Davis, S. J., & Davis, K. A. (2023). Large global variations in the carbon dioxide removal potential of seaweed farming due to biophysical constraints. *Communications Earth & Environment*, 4(1), 185. <https://doi.org/10.1038/s43247-023-00833-2>
- Bailey, B. N., & Stoll, R. (2013). Turbulence in sparse, organized vegetative canopies: A large-eddy simulation study. *Boundary-Layer Meteorology*, 147(3), 369–400. <https://doi.org/10.1007/s10546-012-9796-4>
- Bo, T. (2024). Nutrient transport and uptake in suspended macroalgal farms [Dataset]. Zenodo. <https://doi.org/10.5281/zenodo.10739134>
- Bo, T., McWilliams, J. C., Yan, C., & Chamecki, M. (2024). Langmuir turbulence in suspended kelp farms. *Journal of Fluid Mechanics*, 985, A11. <https://doi.org/10.1017/jfm.2024.287>
- Broch, O. J., & Slagstad, D. (2012). Modelling seasonal growth and composition of the kelp *saccharina latissima*. *Journal of Applied Phycology*, 24(4), 759–776. <https://doi.org/10.1007/s10811-011-9695-y>
- Cornish-Bowden, A. (2015). One hundred years of Michaelis–Menten kinetics. *Perspectives in Science*, 4, 3–9. <https://doi.org/10.1016/j.pisc.2014.12.002>
- Craik, A. D., & Leibovich, S. (1976). A rational model for Langmuir circulations. *Journal of Fluid Mechanics*, 73(3), 401–426. <https://doi.org/10.1017/s0022112076001420>
- Dayton, P. K. (1985). Ecology of kelp communities. *Annual Review of Ecology and Systematics*, 16(1), 215–245. <https://doi.org/10.1146/annurev.ecolsys.16.1.215>
- Deardorff, J. W. (1970). A numerical study of three-dimensional turbulent channel flow at large Reynolds numbers. *Journal of Fluid Mechanics*, 41(2), 453–480. <https://doi.org/10.1017/s0022112070000691>
- Deutsch, C., Frenzel, H., McWilliams, J. C., Renault, L., Kessouri, F., Howard, E., et al. (2021). Biogeochemical variability in the California current system. *Progress in Oceanography*, 196, 102565. <https://doi.org/10.1016/j.pocean.2021.102565>
- Ferdouse, F., Holdt, S. L., Smith, R., Murúa, P., & Yang, Z. (2018). The global status of seaweed production, trade and utilization. *Globefish Research Programme*, 124, 120.
- Fernand, F., Israel, A., Skjermo, J., Wichard, T., Timmermans, K. R., & Golberg, A. (2017). Offshore macroalgae biomass for bioenergy production: Environmental aspects, technological achievements and challenges. *Renewable and Sustainable Energy Reviews*, 75, 35–45. <https://doi.org/10.1016/j.rser.2016.10.046>
- Finnigan, J. (2000). Turbulence in plant canopies. *Annual Review of Fluid Mechanics*, 32(1), 519–571. <https://doi.org/10.1146/annurev.fluid.32.1.519>
- Frieder, C. A., Yan, C., Chamecki, M., Dauhajre, D., McWilliams, J. C., Infante, J., et al. (2022). A macroalgal cultivation modeling system (MACMODS): Evaluating the role of physical-biological coupling on nutrients and farm yield. *Frontiers in Marine Science*, 9, 752951. <https://doi.org/10.3389/fmars.2022.752951>
- Gerard, V. A. (1982). In situ rates of nitrate uptake by giant kelp, *Macrocystis Pyrifera* (L.) C. Agardh: Tissue differences, environmental effects, and predictions of nitrogen-limited growth. *Journal of Experimental Marine Biology and Ecology*, 62(3), 211–224. [https://doi.org/10.1016/0022-0981\(82\)90202-7](https://doi.org/10.1016/0022-0981(82)90202-7)
- Ghadiryfar, M., Rosentrater, K. A., Keyhani, A., & Omid, M. (2016). A review of macroalgae production, with potential applications in biofuels and bioenergy. *Renewable and Sustainable Energy Reviews*, 54, 473–481. <https://doi.org/10.1016/j.rser.2015.10.022>
- Haines, K. C., & Wheeler, P. A. (1978). Ammonium and nitrate uptake by the marine macrophytes *Hypnea Musviformis* (Rhodophyta) and *Macrocystis Pyrifera* (Phaeophyta) 1, 2. *Journal of Phycology*, 14(3), 319–324. <https://doi.org/10.1111/j.1529-8817.1978.tb00305.x>
- Huang, I., Rominger, J., & Nepf, H. (2011). The motion of kelp blades and the surface renewal model. *Limnology & Oceanography*, 56(4), 1453–1462. <https://doi.org/10.4319/lo.2011.56.4.1453>
- Jackson, G. A. (1997). Currents in the high drag environment of a coastal kelp stand off California. *Continental Shelf Research*, 17(15), 1913–1928. [https://doi.org/10.1016/s0278-4343\(97\)00054-x](https://doi.org/10.1016/s0278-4343(97)00054-x)
- McWilliams, J. C., Sullivan, P. P., & Moeng, C.-H. (1997). Langmuir turbulence in the ocean. *Journal of Fluid Mechanics*, 334, 1–30. <https://doi.org/10.1017/s0022112096004375>
- Michaelis, L., & Menten, M. L. (1913). Die kinetik der invertinwirkung. *Biochemische Zeitschrift*, 49(333–369), 352.
- Monismith, S., Alnajjar, M., Daly, M., Valle-Levinson, A., Juarez, B., Fagundes, M., et al. (2022). Kelp forest drag coefficients derived from tidal flow data. *Estuaries and Coasts*, 45(8), 2492–2503. <https://doi.org/10.1007/s12237-022-01098-2>
- Nepf, H., Ghisalberti, M., White, B., & Murphy, E. (2007). Retention time and dispersion associated with submerged aquatic canopies. *Water Resources Research*, 43(4), W04422. <https://doi.org/10.1029/2006wr005362>
- Plew, D. R. (2011). Depth-averaged drag coefficient for modeling flow through suspended canopies. *Journal of Hydraulic Engineering*, 137(2), 234–247. [https://doi.org/10.1061/\(asce\)hy.1943-7900.0000300](https://doi.org/10.1061/(asce)hy.1943-7900.0000300)
- Plew, D. R., Spigel, R. H., Stevens, C. L., Nokes, R. I., & Davidson, M. J. (2006). Stratified flow interactions with a suspended canopy. *Environmental Fluid Mechanics*, 6, 519–539. <https://doi.org/10.1007/s10652-006-9008-1>
- Poggi, D., Porporato, A., Ridolfi, L., Albertson, J., & Katul, G. (2004). The effect of vegetation density on canopy sub-layer turbulence. *Boundary-Layer Meteorology*, 111(3), 565–587. <https://doi.org/10.1023/b:boun.0000016576.0562.1.73>

- Rehage, H., & Kind, M. (2021). The first damköhler number and its importance for characterizing the influence of mixing on competitive chemical reactions. *Chemical Engineering Science*, 229, 116007. <https://doi.org/10.1016/j.ces.2020.116007>
- Renault, L., McWilliams, J. C., Kessouri, F., Jousse, A., Frenzel, H., Chen, R., & Deutsch, C. (2021). Evaluation of high-resolution atmospheric and oceanic simulations of the California current system. *Progress in Oceanography*, 195, 102564. <https://doi.org/10.1016/j.pocean.2021.102564>
- Rosman, J. H., Koseff, J. R., Monismith, S. G., & Grover, J. (2007). A field investigation into the effects of a kelp forest (*Macrocystis Pyrifera*) on coastal hydrodynamics and transport. *Journal of Geophysical Research*, 112(C2), C02016. <https://doi.org/10.1029/2005jc003430>
- Smagorinsky, J. (1963). General circulation experiments with the primitive equations: I. The basic experiment. *Monthly Weather Review*, 91(3), 99–164. [https://doi.org/10.1175/1520-0493\(1963\)091<099:gcewtp>2.3.co;2](https://doi.org/10.1175/1520-0493(1963)091<099:gcewtp>2.3.co;2)
- Stevens, C. L., & Hurd, C. L. (1997). Boundary-layers around bladed aquatic macrophytes. *Hydrobiologia*, 346(1/2/3), 119–128. <https://doi.org/10.1023/a:1002914015683>
- Teagle, H., Hawkins, S. J., Moore, P. J., & Smale, D. A. (2017). The role of kelp species as biogenic habitat formers in coastal marine ecosystems. *Journal of Experimental Marine Biology and Ecology*, 492, 81–98. <https://doi.org/10.1016/j.jembe.2017.01.017>
- Thom, A. (1971). Momentum absorption by vegetation. *Quarterly Journal of the Royal Meteorological Society*, 97(414), 414–428. <https://doi.org/10.1256/smsqj.41403>
- Troell, M., Joyce, A., Chopin, T., Neori, A., Buschmann, A. H., & Fang, J.-G. (2009). Ecological engineering in aquaculture—Potential for integrated multi-trophic aquaculture (IMTA) in marine offshore systems. *Aquaculture*, 297(1–4), 1–9. <https://doi.org/10.1016/j.aquaculture.2009.09.010>
- Tseung, H. L., Kikkert, G. A., & Plew, D. (2016). Hydrodynamics of suspended canopies with limited length and width. *Environmental Fluid Mechanics*, 16(1), 145–166. <https://doi.org/10.1007/s10652-015-9419-y>
- Utter, B. D., & Denny, M. W. (1996). Wave-induced forces on the giant kelp *Macrocystis Pyrifera* (Agardh): Field test of a computational model. *Journal of Experimental Biology*, 199(12), 2645–2654. <https://doi.org/10.1242/jeb.199.12.2645>
- Yan, C., McWilliams, J. C., & Chamecki, M. (2021). Generation of attached Langmuir circulations by a suspended macroalgal farm. *Journal of Fluid Mechanics*, 915, A76. <https://doi.org/10.1017/jfm.2021.111>
- Yan, C., McWilliams, J. C., & Chamecki, M. (2022). Overlapping boundary layers in coastal oceans. *Journal of Physical Oceanography*, 52(4), 627–646. <https://doi.org/10.1175/jpo-d-21-0067.1>
- Zimmerman, R. C., & Kremer, J. N. (1984). Episodic nutrient supply to a kelp forest ecosystem in southern California. *Journal of Marine Research*, 42(3), 591–604. <https://doi.org/10.1357/002224084788506031>